

ORIGINAL ARTICLE

Open Access



# Design and Experiment of Triangular Prism Mast with Tape-Spring Hyperelastic Hinges

Hui Yang<sup>1</sup> , Hong-Wei Guo<sup>2\*</sup> , Yan Wang<sup>3</sup>, Rong-Qiang Liu<sup>2</sup> and Meng Li<sup>4</sup>

## Abstract

Because of the limited space of the launch rockets, deployable mechanisms are always used to solve the phenomenon. One dimensional deployable mast can deploy and support antenna, solar sail and space optical camera. Tape-spring hyperelastic hinges can be folded and extended into a rod like configuration. It utilizes the strain energy to realize self-deploying and drive the other structures. One kind of triangular prism mast with tape-spring hyperelastic hinges is proposed and developed. Stretching and compression stiffness theoretical model are established with considering the tape-spring hyperelastic hinges based on static theory. The finite element model of ten-module triangular prism mast is set up by ABAQUS with the tape-spring hyperelastic hinge and parameter study is performed to investigate the influence of thickness, section angle and radius. Two-module TPM is processed and tested the compression stiffness by the laser displacement sensor, deploying repeat accuracy by the high speed camera, modal shape and fundamental frequency at cantilever position by LMS multi-channel vibration test and analysis system, which are used to verify precision of the theoretical and finite element models of ten-module triangular prism mast with the tape-spring hyperelastic hinges. This research proposes an innovative one dimensional triangular prism with tape-spring hyperelastic hinge which has great application value to the space deployable mechanisms.

**Keywords:** Deployable mechanism, Triangular prism mast, Tape-spring hyper-elastic hinges, Static analysis, Modal experiment

## 1 Introduction

Conventional articulated truss structures are composed of mechanical hinges which can meet accuracy and stiffness requires of space mission. But those structures have some disadvantages, such as large weight, high friction and energy-wasting features. Tape-spring hyperelastic (TSH) hinges, which are folded elastically can self-deploy by releasing stored strain energy, which consist of a fewer component parts, can be manufactured conveniently [1, 2]. Flexible hinges have several advantages for space applications, including a low mass-to-deployed-stiffness ratio, cost, and self-latch [3]. With the increasing demand, flexible hinges have been widely used as folding

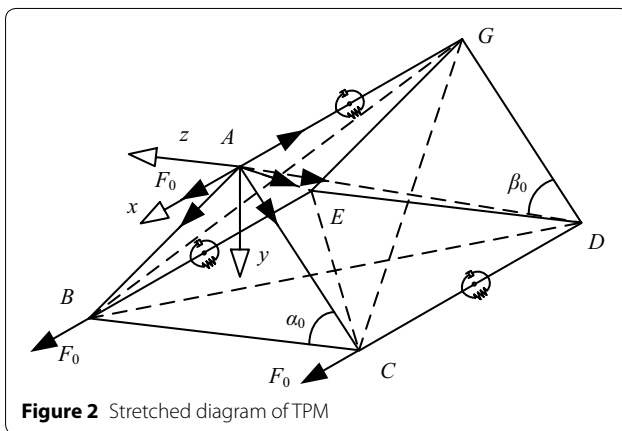
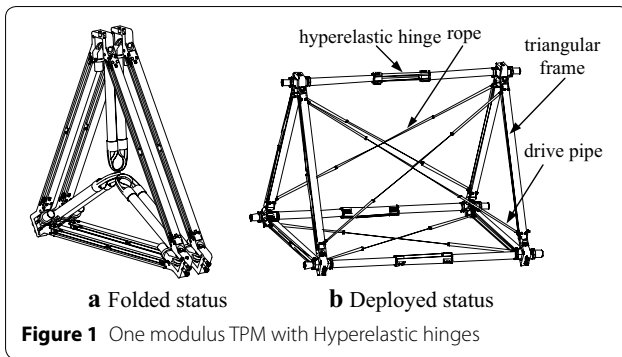
and deployment mechanisms in deployable structures, such as synthetic aperture radars (SARs) [4–6], solar arrays and antenna booms. Tape-spring hinges have been used in the Japanese Mars orbiter PLANET-B for bar-like deployment structures of the thermal plasma analyzer [7–9].

The U.S. Air Force Research Laboratory (AFRL) [10] used TSH hinge in the main truss's folding longeron elements, which provided considerable snap-through force to drive and lock the main truss. Imperial College London Santer [11] proposed a concertina-folded magnetometer boom with TSH hinges for CubeSat use. Watt et al. [12] proposed a TSH hinge with two sets of wheels held together by wires wrapped around them, and deploying impact is reduced for the added damp. The Mars Advanced Radar Express spacecraft [13, 14] consisted of two 20 m dipoles and a 7 m monopole which were slotted at certain intervals to stow them in a much

\*Correspondence: guohw@hit.edu.cn

<sup>2</sup> China State Key Laboratory of Robotics and System, Harbin Institute of Technology, Harbin 150001, China

Full list of author information is available at the end of the article



small size. Silver et al. [15] proposed an integral folding hinge to deploy camera and investigated axial loading, bending induced buckling response. Schioler et al. and Seffen et al. [16, 17] analyzed buckling properties of single layer TSH hinge based on Timoshenko theory. Seffen et al. [18] got sample points by finite element method and obtained fitting nonlinear mechanical models by single value decomposition method of TSH hinge. Guan et al. [19, 20] designed a TSH hinge for solar sail and investigated its buckling properties by finite element method. Bai et al. [21], Yan et al. [22], Wang et al. [23] investigated geometrical and mechanical properties of ultra-thin-walled lenticular collapsible composite tube in fold deformation. Yang et al. [24, 25] optimized the geometric parameters of TSH hinge to improve driving moment and reduce deploying impact, and established two different theoretical models to analyze the stability of deployment status for the TSH hinges. However, there are still some engineering problems for the TSH hinge applying to a deployable mechanism.

This paper proposed a new ten-module triangular prism mast (TPM) with TSH hinges. Static bending stiffness and compression stiffness theoretical models are established. The compression stiffness tests

are performed to verify the accuracy of the static theoretical models of the TPM. Finite element model of ten-module TPM are established by ABAQUS and geometrical parameter study are analyzed for bending and twisted modal frequencies. Two-module TPM is developed to test the fundamental frequencies and related modal shapes which are used to verify the accuracy of the ten-module TPM (Additional file 1).

## 2 Design and Static Analysis

### 2.1 Structures Design

One module TPM with tape-spring hinges is shown in Figure 1. Adjacent two-module is connected by triangular frame. The length of triangular frame is 469 mm, stowed and deployed longitudinal lengths of ten-module prism mast are 475.2 mm and 5278 mm respectively. All components except standard parts are manufactured by duralumin 2A12. Each modulus TPM with TSH hinge contains three longitudinal links and two triangular frames. The TSH hinges are used to drive and lock TPM. Lateral area of each modulus has a series of flexible Kevlar rope with tensile force 30 N which ensures high stiffness of the deployed prism mast and reduces deploying impact. There is one resin-based carbon fiber drive pipe one each end of the tensile lock which prevent involvement during deploying process.

The TSH hinge folded with 180°, the two triangular frame close to each other, and three longitudinal links folded between the two triangular frames when the mast stowed. The tape-spring drive the mast to deploy. After deploying, the TSH hinge restore original shape, the Kevlar ropes tensile and the TPM was rigidified to a structure.

### 2.2 Static Analysis

Bending stiffness analysis has been analyzed in Ref. [8]. Thus, stretching stiffness and compression stiffness will be derived in this paper.

#### 2.2.1 Stretching Stiffness

Axial force  $F_0$  is applied on each point  $A$ ,  $B$  and  $C$ . Circumcircle radius of cross section is  $R_1 = l_b / \sqrt{3}$ . Stretch force diagram is shown as Figure 2.

By resolving the forces in the  $x$ -direction at point  $A$ , the equation is obtained as follows.

$$2F_{r0} \sin \beta_0 + F_l = F_0, \tag{1}$$

where  $F_l$  is axial force of longitudinal link,  $F_{r0}$  is initial pretension of the rope,  $l_b$  is the cross link length,  $\beta_0$  is the angle between line  $GD$  and line  $ED$ .

When the TPM is under stretching, deformation of longitudinal link and diagonal rope has following related equation based on geometric deformation condition.

$$\delta_r^i = \delta_l^i \sin \beta_0, \tag{2a}$$

$$\delta_r^i = \frac{F_r l_r}{E_r A_r}, \tag{2b}$$

$$\delta_l^i = \frac{2F_l l_1}{E_1 A_1} + \frac{F_l l_2}{n_1 a_{11}}, \tag{2c}$$

where  $\delta_r^i$  is rope deformation in each modulus,  $\delta_l^i$  is longitudinal stretch deformation of each modulus,  $l_r$  is rope length,  $F_r$  is the force in rope,  $E_r$  is the material Young modulus for rope,  $A_r$  is cross section area of the rope,  $l_1$  is the length of longitudinal rigid link,  $l_2$  is the length of the TSH hinge,  $F_l$  is the force in the longitudinal link,  $E_1$  is the material Young modulus for longitudinal link,  $A_1$  is the cross-section area of the longitudinal link,  $n_1$  is the number of the tape spring,  $a_{11}$  is the unit stretching stiffness of the TSH hinge.

Stretch deformation  $\delta_l$  of the TPM is

$$\delta_l = \frac{n_2 \cdot 3F_0(2l_1 + l_2)}{EA}, \tag{3a}$$

$$\delta_l = n_2 \delta_l^i, \tag{3b}$$

where  $n_2$  is the module number of the TPM,  $EA$  is the stretching stiffness of the TPM.

Simultaneous Eqs. (1), (2) and (3), stretching stiffness of the TPM is obtained as follows:

$$EA = 6E_r A_r \sin^3 \beta_0 + \frac{3(2l_1 + l_2)}{\frac{2l_1}{E_1 A_1} + \frac{l_2(1-\nu^2)}{n_1 E t}}. \tag{4}$$

If the TPM has no rope, the stretching stiffness is rearranged as follows:

$$EA = \frac{3(2l_1 + l_2)}{\frac{2l_1}{E_1 A_1} + \frac{l_2(1-\nu^2)}{n_1 E t}}.$$

### 2.2.2 Compression Stiffness

One end of the TPM is fixed and a compressive force  $3F_0$  is applied on the other end. Due to initial tension  $F_{r0}$  of rope initial deformation is  $\delta_{r0} = F_{r0} l_r / (E_r A_r)$ , which leads to a critical compress value  $3F_0'$  on the end. Based on the geometric deformation conditions longitudinal link deformation of each module is written as follows:

$$\delta_l^i = \frac{\delta_{r0}}{\sin \beta_0}. \tag{5}$$

When compressive force is applied at point  $A$ , equilibrium equation is gotten as follows:

$$-2F_r \sin \beta_0 + F_l = F_0. \tag{6}$$

Simultaneous Eq. (2c), Eq. (5) and Eq. (6), critical unloaded compressive force is expressed as follows:

$$F' = \frac{3F_{r0} l_r}{E_r A_r \sin \beta_0 \left( \frac{2l_1}{E_1 A_1} + \frac{l_2}{n_1 a_{11}} \right)}. \tag{7}$$

If axial compressive force is no less than the critical unloaded compressive force, unloaded compressive stiffness equals to sum total compression stiffness of longitudinal rigid links and hyperelastic tape-spring hinges, that is

$$EA = \frac{3(2l_1 + l_2)}{\frac{2l_1}{E_1 A_1} + \frac{l_2}{n_1 a_{11}}}. \tag{8}$$

If axial compressive force is more than the critical unloaded compressive force, the total deformation of the rope is

$$\delta_r = \delta_{r0} - \delta_r', \tag{9a}$$

$$\delta_r' = \frac{F_r' l_r}{E_r A_r}, \tag{9b}$$

where  $\delta_r'$  is deformation of the rope with only axial compress force,  $\delta_{r0}$  is deformation of the rope under initial pretension force.

Single module longitudinal link and rope deformation meets the geometric deformation conditions. When  $3F_0$  is lower than  $F'$ , simultaneous Eq. (2), Eq. (3), Eq. (6) and Eq. (9) equivalent compression stiffness of the TPM is

$$EA = 6E_r A_r \sin^3 \beta_0 + 3 \left( 1 - \frac{2F_{r0} \sin \beta_0}{F_l'} \right) \frac{(2l_1 + l_2)}{\frac{2l_1}{E_1 A_1} + \frac{l_2(1-\nu^2)}{n_1 E t}}. \tag{10}$$

It is found that when  $3F_0$  is more than  $F'$  the compression stiffness is related to the compression stiffness of the longitudinal link and the TSH hinges; when  $3F_0$  is lower than  $F'$ , the compression stiffness changed with axial load. If the end compress load  $3F_0$  is much small, that is

$$3F_0 = 12F_0 \sin^3 \beta_0 \cdot \left[ \frac{2l_1}{E_1 A_1} + \frac{l_2(1-\nu^2)}{n_1 E t} \right] \cdot \frac{E_r A_r}{l_r}. \tag{11}$$

The compression stiffness can be written as follows

$$EA = 6E_r A_r \sin^3 \beta_0. \tag{12}$$

The compression stiffness is only related to the rope stiffness  $E_r A_r$  and initial angle  $\beta_0$ .

### 3 Deploying State Modal Analysis

#### 3.1 Modal Analysis

Due to nonlinear characteristics of the TSH hinge modal analysis of the TPM is performed by ABAQUS. In finite element model  $x$ -axis is along direction of transverse link,  $y$ -axis is along longitudinal link and  $z$ -axis points from section center of transverse links to point of the other two transverse links. Materials of the TSH hinge, rigid link, transverse link and rope are Ni36CrTiAl, stainless steel, aluminum alloy and Kevlar respectively. Longitudinal link, transverse link and the TSH hinge are set up with four nodes that are fully integrated to reduce shell elements (S4R). Rope is modeled by two nodes and three dimensional elements (T3D2). Weld is defined to model connection between ropes and transverse links. Reference point (RP) is established at each joint which are given mass and inertial properties. Multi-point coupling is applied to model the connection of transverse links. The joint hinges are modeled by defining Hinge connection. Contact of tape springs are modeled by defining Tie constraint.

Six reference points at the root of the TPM restrain three translational Degree of Freedoms (DOFs) and the TPM is in the state of cantilever. Firstly, the TPM is performed on static analysis with 30 N pretension force and deformation is got. Then, modal analysis is done by subspace method with rope prestress deformation. Total length for ten-module TPM is 5.26 m. Figure 3 shows the FEM of the ten-module TPM with TSH hinges.

The five order modal shapes of ten modules TPM with TSH hinge are shown in Figure 4. The five order mode frequencies and mode shape description are listed in Table 1.

#### 3.2 Parameter Study

Compared to conventional rigid deployable mechanism the TSH hinge introduces flexible influence. Thus, it is necessary to analyze the effect of geometric parameters, such as thickness  $t$ , cross-section radius  $R$ , center angle  $\phi$  and separation distance  $s$ , to mode frequency and propose method of increasing stiffness. Table 2 lists frequencies of ten-module TPM under different thickness. It is shown that bend frequency increases 3.695%–11.84% and twist frequency increases 0.186%–0.221% when the thickness changes from 0.12 mm to 0.14 mm.

Table 3 lists ten-module mast frequencies under different tape central angles. It can be seen that the bend frequency increases by 3.654%–6.156% and twist frequency increases by 0.393%–0.434% when the central angle changes from 80° to 100°.

Frequencies of the ten-module TPM under different radiuses are listed in Table 4. It can be seen that bend frequencies increase by 2.674%–5.343% and twist

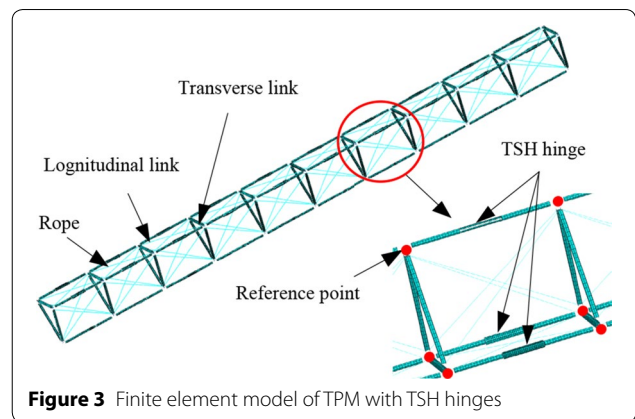


Figure 3 Finite element model of TPM with TSH hinges

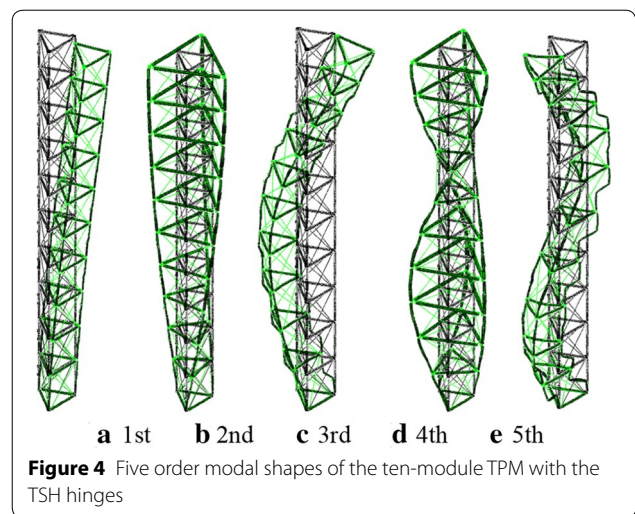


Figure 4 Five order modal shapes of the ten-module TPM with the TSH hinges

Table 1 Five order mode frequencies and mode shape description of the ten-module TPM with TSH hinges

Order	1	2	3	4	5
Frequency (Hz)	2.561	4.243	9.770	12.671	19.557
Model shape	Bend	Twist	Bend	Twist	Bend

Table 2 Frequencies of ten-module TPM under different thicknesses

Frequency (Hz)	Thickness $t$ (mm)			Variable quantity $\delta$ (%)
	0.12	0.16	0.20	
$f_{B1}$	2.5699	2.7468	2.8742	-11.84
$f_{B2}$	9.7959	10.124	10.361	-5.769
$f_{B3}$	19.593	20.018	20.317	-3.695
$f_{T1}$	4.2444	4.2488	4.2523	-0.186
$f_{T2}$	12.674	2.690	12.702	-0.221

**Table 3** Frequencies of ten-module TPM under different tape central angles

Frequency (Hz)	Angle $\varphi$ (°)			Variable quantity $\delta$ (%)
	80	90	100	
$f_{B1}$	2.5699	2.6553	2.7281	-6.156
$f_{B2}$	9.7959	10.022	10.208	-4.207
$f_{B3}$	19.593	20.002	20.309	-3.654
$f_{T1}$	4.2444	4.253	4.2611	-0.393
$f_{T2}$	12.674	12.702	12.729	-0.434

**Table 4** Frequencies of ten-module TPM under different radiuses

Frequency (Hz)	Radius $R$ (mm)			Variable quantity $\delta$ (%)
	18	20	22	
$f_{B1}$	2.5699	2.6433	2.7072	-5.343
$f_{B2}$	9.7959	9.9694	10.118	-3.288
$f_{B3}$	19.593	19.889	20.117	-2.674
$f_{T1}$	4.2444	4.2525	4.2602	-0.372
$f_{T2}$	12.674	12.701	12.726	-0.41

frequencies increase by 0.372%–0.41% when radius change from 18 mm to 22 mm.

Frequencies of ten-module TPM under different separations are listed in Table 5. It can be seen that bend frequencies decrease by 0.0428%–0.0919% and twist frequencies increase by 0.134%–0.141% when the separation changes from 16 mm to 20 mm.

It can be concluded that geometric parameters have greater influence on bend stiffness than twist stiffness. Sensitivity of the geometric parameter is from large to small as follows: thickness, central angle, radius and separation. What’s more, front three parameters have enhanced effect on bend stiffness and the last one has induced effect.

**4 Experiment Investigation**

**4.1 Two-module TPM**

To validate the precision of static stiffness theoretical model, two units triangular prism mast is developed. Figure 5 is folding and deployment configurations of triangular prism mast with hyperelastic hinges.

Two adjacent units triangular prism mast are closed to each other by locating pins and fastened to a work holder by a rope when it is folded. At this time, the longitudinal links are stowed into the prism frames and tension ropes are located to grooves. After releasing the tension ropes,

**Table 5** Frequencies of ten-module TPM under different separations

Frequency (Hz)	Separation $s_e$ (mm)			Variable quantity $\delta$ (%)
	16	18	20	
$f_{B1}$	2.5699	2.5688	2.5688	0.0428
$f_{B2}$	9.7959	9.7866	9.7869	0.0919
$f_{B3}$	19.593	19.582	19.583	0.051
$f_{T1}$	4.2444	4.2468	4.2504	-0.141
$f_{T2}$	12.674	12.681	12.691	-0.134

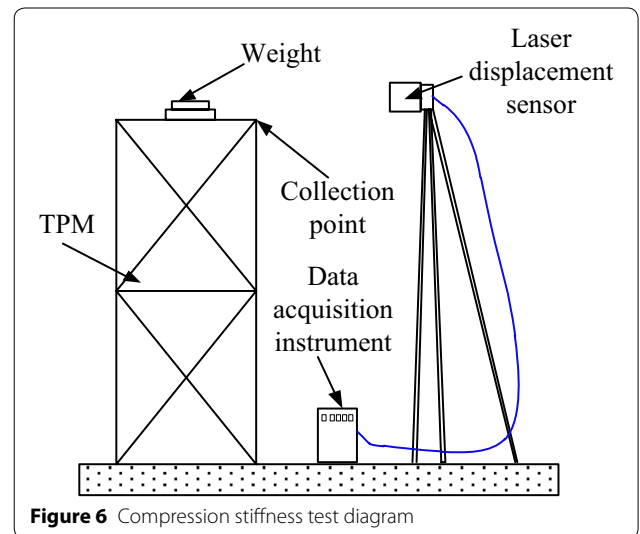
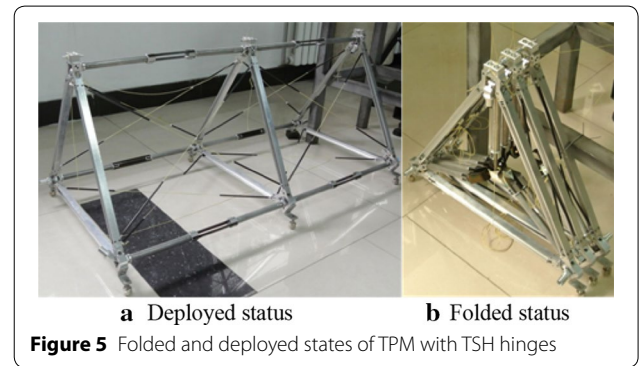


**Table 6** Compress load and displacement for the two-modulus TPM

Load (N)	100	200	300	400	500
Displacement (mm)	0.0168	0.0720	0.1092	0.1895	0.2532

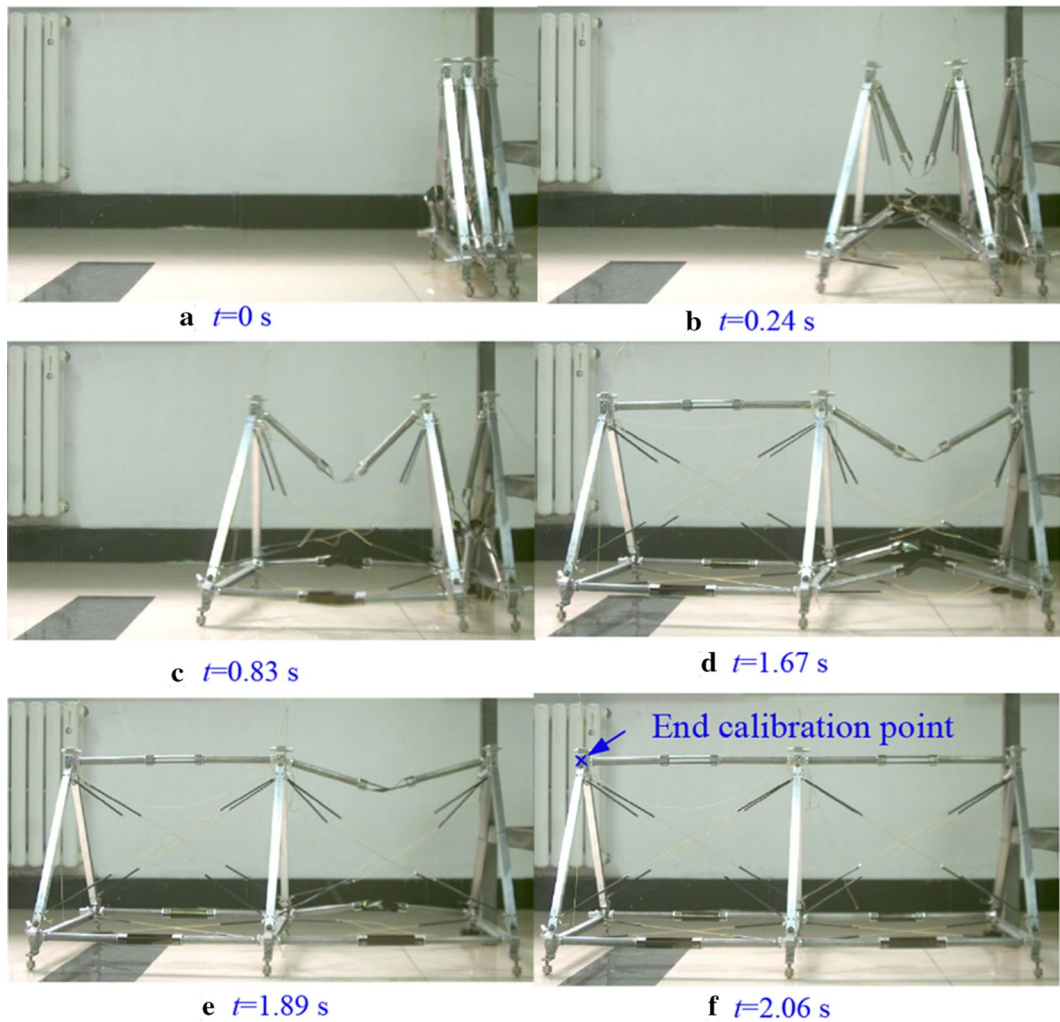


**Figure 7** Deploying configuration for the two-modulus TPM

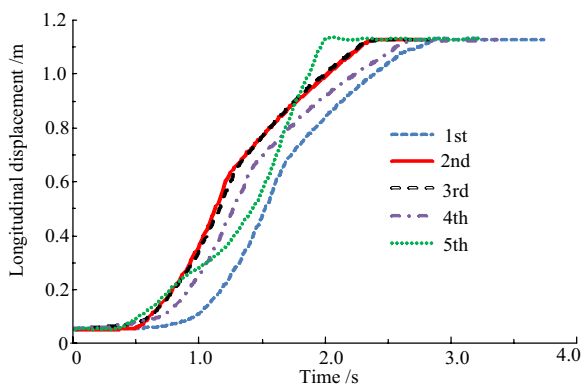


**Figure 8** Longitudinal displacement–time relationship for five times deploying processes

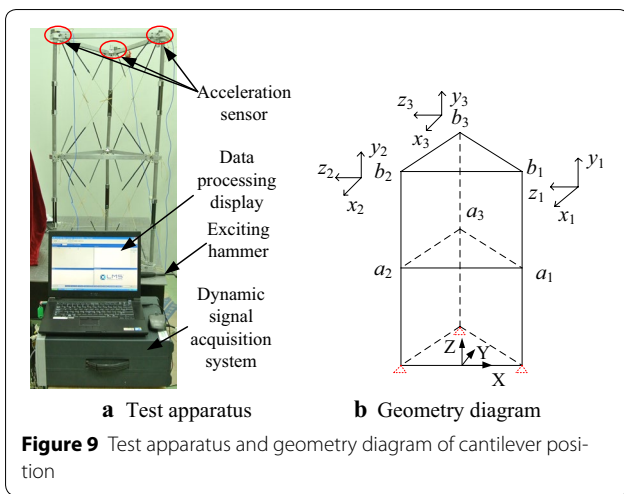
**Table 7** Longitudinal displacement for five times deployment

Number	1	2	3	4	5
Displacement (mm)	1059.755	1055.55	1057.311	1056.98	1059.073

the triangular prism mast is deploying by the driving of the TSH hinges. Spherical wheels support the mast to reduce the influence of gravity.

**4.2 Compression Stiffness Test**

Figure 6 is compression stiffness test diagram of the TPM. Weights are applied at the end of the TPM for 10 kg at each time. Compress load and displacement for the two-modulus TPM are listed in Table 6.



It can be calculated that experimental compression stiffness is  $2.324 \times 10^6$  N/m and theoretical value is  $2.167 \times 10^6$  N/m. Relative error between the experimental and theoretical value is 7.08%. The main reason for the phenomenon is that equivalent stiffness of the TSH hinges is much smaller, contact stiffness between the tape springs should be considered.

### 4.3 Deploying Repeat Accuracy Test

Figure 7 shows deploying configuration for the two modulus TPM. High-speed camera is employed to capture deploying process of the TPM. Spherical hinges and elastic rope are used to eliminate the effect of weight and friction. Figure 8 shows longitudinal displacement-time relationship for five times deploying processes. Table 7 lists compress load and displacement for the two-modulus TPM.

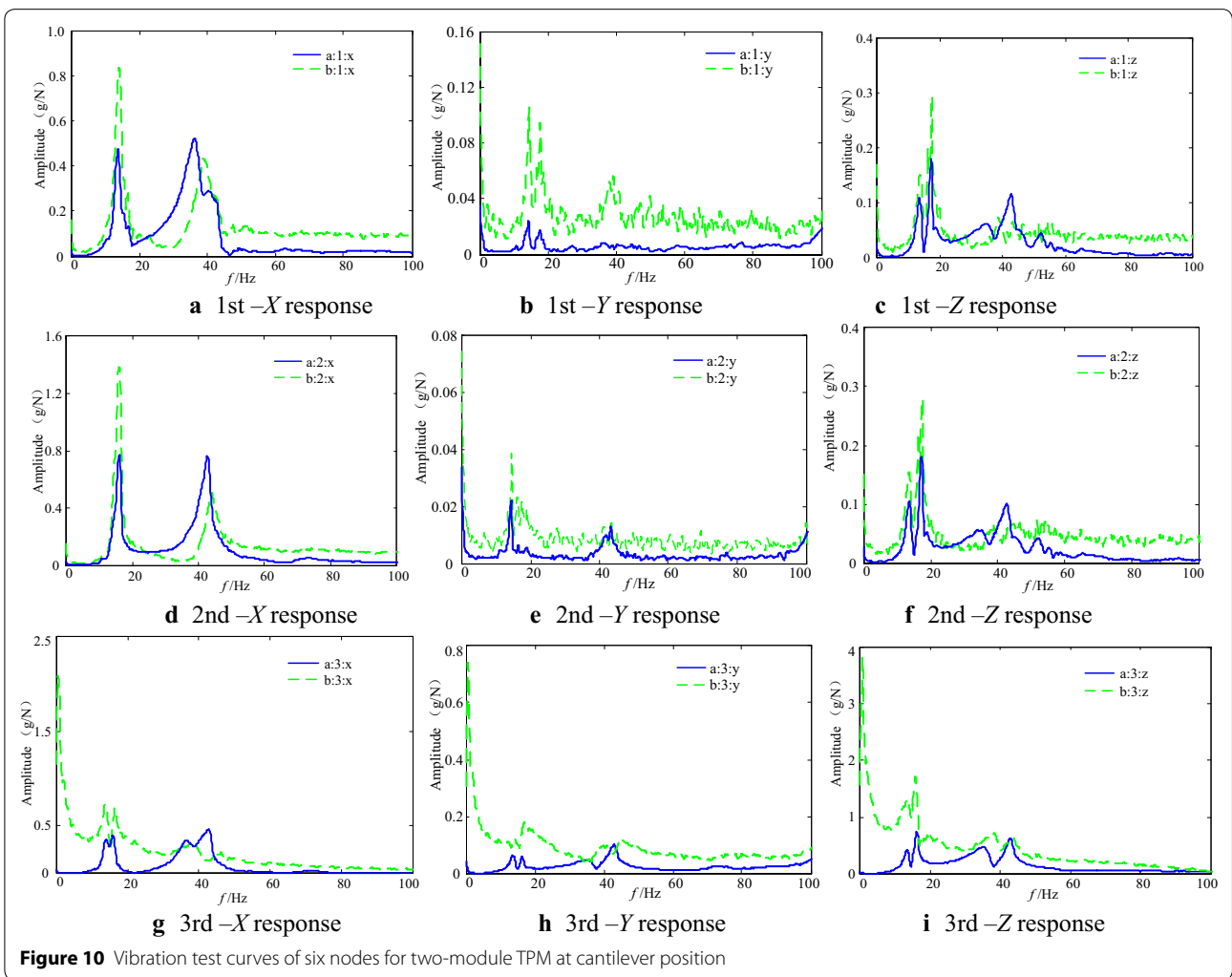


Figure 10 Vibration test curves of six nodes for two-module TPM at cantilever position

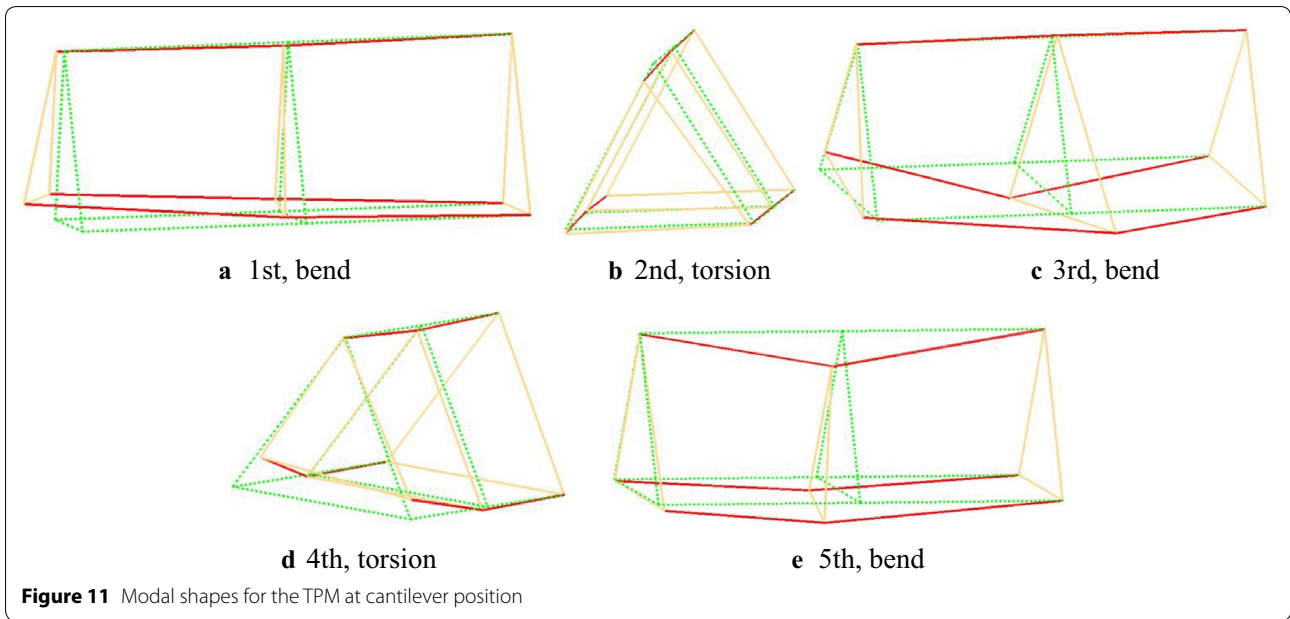


Figure 11 Modal shapes for the TPM at cantilever position

Table 8 Modal test results for the two-modulus TPM at cantilever position

	1st	2nd	3rd	4th	5th
Frequency $f$ (Hz)	13.020	15.743	35.441	39.006	42.744
Mode shape	bend	twist	bend	twist	bend

Based on longitudinal displacement for five times deploying test standard deviation of the experimental value is 1.688 mm. Thus, deploying repeat accuracy is 1.688 mm.

#### 4.4 Modal Analysis of Cantilever Position

LMS multi-channel vibration test and analysis system is employed to measure fundamental frequencies and mode shapes which consists of exciting hammer, acceleration sensor which can test three directional accelerations, dynamic signal acquisition system and data processor. The longitudinal direction of the TPM is set as  $x$ -axis, outer normal direction of cross section is set as  $y$ -axis and vertical downward direction is set as  $z$ -axis which is selected as force hammer stimulating direction. The measurements of three acceleration sensors, which are located at three nodes on the crossbeam, are divided into three groups. Then, integral modal superposition is carried out. The exciting point is set at one end of the cross-beam. Test apparatus and geometry diagram of cantilever position are shown in Figure 9. Three vertexes on the bottom are constrained points. Alphabets  $a$  and  $b$  stand for the order of two times measurement. Location of point  $b_3$  is closest to the exciting point. Vibration test curves of six nodes for two-module TPM at cantilever position are shown in Figure 10. Modal shapes for the TPM at cantilever position are shown in Figure 11. Modal test results for the two-modulus TPM at cantilever position are listed in Table 8. It can be seen that acceleration sensor at point  $b_3$  has a larger response at initial phase; response curves of two group acceleration sensors are concentrated on

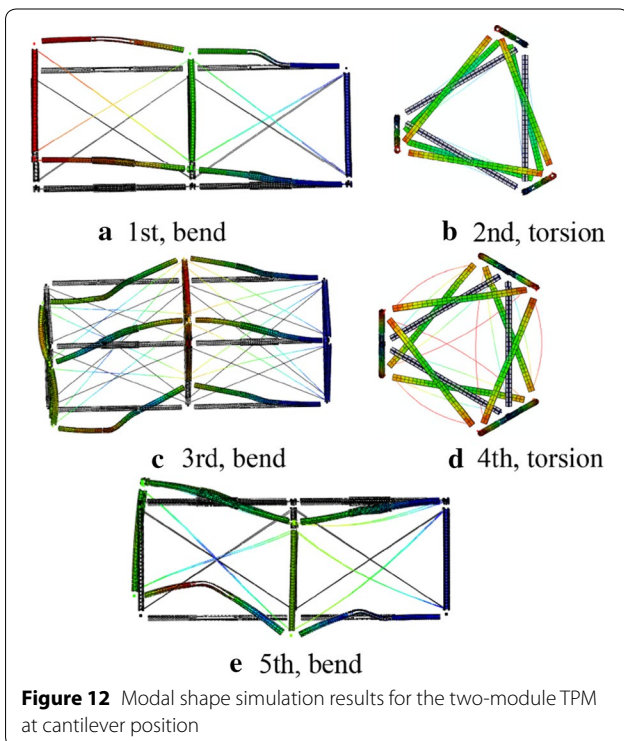


Figure 12 Modal shape simulation results for the two-module TPM at cantilever position



**Table 9 Comparison between modal test and simulation results for the two-modulus TPM at cantilever position**

	1st	2nd	3rd	4th	5th
Experiment value	13.020	15.743	35.441	39.006	42.744
Simulation value	13.732	14.877	34.754	39.612	44.850
RE (%)	-5.469	5.501	1.938	1.554	-4.927

middle- and low frequency. The first order frequency of the TPM at cantilever position is 13.02 Hz and corresponding mode shape is bending.

Then, modal analysis of the two-module TPM at cantilever position and the modeling method is identical to the ten-module TPM by ABAQUS. Modal shape simulation results for the two-module TPM at cantilever position are shown in Figure 12.

The model with black lines is undeformed configuration and the model with colored lines is deformed configuration. Comparison between modal test and simulation results for the two-modulus TPM at cantilever position is listed in Table 9. It can be seen that the mode shapes between simulated and experimental results are consistent compared to Figures 11, 12 and Table 9. The relative errors between simulated and experimental results for frequencies are no more than 5.501%. It indicates that the finite element model for the ten-module TPM is accurate.

## 5 Conclusions

Structure design and deploying modal analysis of the ten-modulus TPM are performed. The two-modulus TPM is processed and its mechanical properties are investigated by experiment.

- (1) The experimental and theoretical compression stiffness static models are  $2.324 \times 10^6$  N/m and theoretical value is  $2.167 \times 10^6$  N/m. It verifies the accuracy of the static theoretical models.
- (2) Geometric parameters have greater influence on bend stiffness than twist stiffness. Sensitivity of the geometric parameter is from large to small as follows: thickness, central angle, radius and separation.
- (3) The deploying repeat accuracy of the two-module TPM is 1.688 mm which is tested by the high-speed camera.
- (4) The veracity of the finite element model of the ten-module TPM at cantilever position is validated by modal test of the two-module TPM. The first fundamental frequency of the ten-module TPM is 2.561 Hz and the corresponding mode shape is bending.

## Additional file

**Additional file 1.** Brief introduction of the manuscript.

### Authors' Contributions

H-WG and R-QL was in charge of the whole trial; HY wrote the manuscript; YW and ML assisted with sampling and laboratory analysis. All authors have read and approved the final manuscript.

### Author details

<sup>1</sup> College of Electrical Engineering and Automation, Anhui University, Hefei 230601, China. <sup>2</sup> China State Key Laboratory of Robotics and System, Harbin Institute of Technology, Harbin 150001, China. <sup>3</sup> China Electronics Technology Group Corporation No.38 Research, Hefei 230088, China. <sup>4</sup> Qian Xuesen Laboratory of Space Technology, China Academy of Space Technology, Beijing 100094, China.

### Authors' Information

Hui Yang, born in 1986, is currently a lecturer at *College of Electrical Engineering and Automation, Anhui University, Hefei, China*. She got the doctor degree from *Harbin Institute of Technology, China*, in 2015. Her research interest includes deployable mechanism, membrane antenna, triangular rollable and collapsible boom, tape-spring hyperelastic hinge, multiobjective optimization design, deployment dynamics and finite element analysis. E-mail: huiyang\_0431@163.com.

Hong-Wei Guo, born in 1980, is currently an associate professor at *Harbin Institute of Technology, China*. His main research interest includes space manipulator system vibration control, large deployable structure and energy absorber optimization. E-mail: guohw@hit.edu.cn.

Yan Wang, born in 1986, is currently a senior engineer at *China Electronics Technology Group Corporation No.38 Research, Hefei, China*. His research interest includes configuration synthesis and design of deployable truss structures. E-mail: wangyan\_597@163.com.

Rong-Qiang Liu, born in 1965, is currently a professor at *Harbin Institute of Technology, China*. His main research interest includes wearing robot, military civil power robot and large deployable structure research. E-mail: liurq@hit.edu.cn.

Meng Li, born in 1985, is currently a senior engineer at *Qian Xuesen Laboratory of Space Technology, China Academy of Space Technology*. He got the doctor degree from Harbin Institute of Technology in 2013. His main research interest includes the optimization design of energy-absorber structures, impact dynamics and finite element method. E-mail: limeng@qxslab.cn.

### Competing Interests

The authors declare that they have no competing interests.

### Ethics Approval and Consent to Participate

Not applicable.

### Funding

Supported by National Natural Science Foundation of China (Grant No. 51605001), Joint Funds of the National Natural Science Foundation of China (Grant No. U1637207), and Anhui University Research Foundation for Doctor (Grant No. J01003222).

### Publisher's Note

Springer Nature remains neutral with regard to jurisdictional claims in published maps and institutional affiliations.

Received: 22 June 2017 Accepted: 17 April 2018

Published online: 06 May 2018

### References

- [1] K A Seffen. On the behavior of folded tape-springs. *Journal of Applied Mechanics-Transactions of the ASME*, 2001, 68(3): 369–375.

- [2] J Block, M Straubel, M Wiedemann. Ultralight deployable booms for solar sails and other large gossamer structures in space. *Acta Astronautica*, 2011, 68 (7–8): 984–992.
- [3] M Mobrem, D S Adams. Deployment analysis of the lenticular jointed antennas onboard the Mars express spacecraft. *Journal of Spacecraft and Rockets*, 2009, 46(2): 394–402.
- [4] K Oya, J Onoda. Characteristics of carpenter tape hinge made of TiNi alloy. *Proceedings of the 43rd AIAA/ASME/ASCE/AHS/ASC Structures, Structural Dynamics, and Materials Conference*, Denver, Colorado, April 22–25, 2002.
- [5] H M Y C Mallikarachchi, S Pellegrino. Quasi-static folding and deployment of ultrathin composite tape-spring hinges. *Journal of Spacecraft and Rockets*, 2011, 48(1): 187–198.
- [6] Y Wang, R Q Liu, H Yang, et al. Design and deployment analysis of modular deployable structure for large antennas. *Journal of Spacecraft and Rockets*, 2015, 52(4): 1101–1110.
- [7] Y Wang, H W Guo, H Yang, et al. Deployment analysis and optimization of a flexible deployable structure for large synthetic aperture radar antennas. *Proceedings of the Institute of Mechanical Engineers Part G Journal of Aerospace Engineering*, 2016, 230(4): 615–627.
- [8] H M Y C Mallikarachchi, S Pellegrino. Deployment dynamics of ultrathin composite booms with tape-spring hinges. *Journal of Spacecraft and Rockets*, 2014, 52(2): 604–613.
- [9] B Zi, Y Li. Conclusions in theory and practice for advancing the applications of cable-driven mechanisms. *Chinese Journal of Mechanical Engineering*, 2017, 30(4): 763–765.
- [10] H G Yang, L Ding, H B Gao, et al. Experimental study and modeling of wheel's steering singkage for planetary exploration rovers. *Journal of Mechanical Engineering*, 2017, 53(8): 99–108. (in Chinese)
- [11] M Santer, A Sim, J Stafford. Testing of a segmented compliant deployable boom for CubeSat Magnetometer Missions. *Proceedings of the 52nd AIAA/ASME/ASCE/AHS/ASC Structures, Structural Dynamics, and Materials Conference*, Denver, Colorado, April 4–7, 2011.
- [12] A M Watt, S Pellegrino. Tape-spring rolling hinges. *Proceedings of the 36th Aerospace Mechanisms Symposium, Glenn Research Center*, May 15–17, 2002: 1–14.
- [13] D S Adams, M Mobrem. Lenticular jointed antenna deployment anomaly and resolution onboard the mars express spacecraft. *Journal of Spacecraft and Rockets*, 2009, 46(2): 403–410.
- [14] M Mobrem, D S Adams. Deployment analysis of lenticular jointed antennas onboard the mars express spacecraft. *Journal of Spacecraft and Rockets*, 2009, 46(2): 394–402.
- [15] M J Silver, P Warren. Dynamic modeling of the folding of multi-shell flexible composites. *Proceedings of the 51st AIAA/ASME/ASCE/AHS/ASC Structures, Structural Dynamics, and Materials Conference*, Orlando, Florida, April 12–15, 2010.
- [16] T Schioler, S Pellegrino. A bistable structural element. *Proceedings of the Institute of Mechanical Engineers Part C Journal of Engineering Sciences*, 2008, 222: 2045–2051
- [17] K A Seffen, S Pellegrino. Deployment dynamics of tape springs. *Proceedings of the Royal Society of London Series A*, 1999, 455(1983): 1003–1048.
- [18] K A Seffen, Z You, S Pellegrino. Folding and deployment of curved tape spring. *International Journal of Mechanical Sciences*, 2000, 42: 2055–2073.
- [19] F L Guan, X Y Wu, Y W Wang. The mechanical behavior of the double piece of tape spring. *Proceedings of the 6th International Conference on Intelligent Computing*, Changsha, China, August 18–21, 2010: 102–110.
- [20] J Wang, F L Guan, Z Z Zhou. Design and analysis of tape hinge for deployable structures. *Journal of Astronautics*. 2007, 28(3): 720–726. (in Chinese)
- [21] J B Bai, J J Xiong, J P Gao, et al. Analytical solutions for predicting in-plane strain and interlaminar shear stress of ultra-thin-walled lenticular collapsible composite tube in fold deformation. *Composite Structures*, 2013, 97(2): 64–75.
- [22] Y Yan, H B Wang, Q Li, et al. Finite element simulation of flexible roll forming with supplemented material data and the experimental verification. *Chinese Journal of Mechanical Engineering*, 2016, 29(2): 342–350.
- [23] W Wang, P Y Lian, S X Zhang, et al. Effect of facet displacement on radiation field and its application for panel adjustment of large reflector antenna. *Chinese Journal of Mechanical Engineering*, 2017, 30(3): 578–586.
- [24] H Yang, H W Guo, Y Wang, et al. Mechanical modeling and analysis for hyperelastic hinge in a triangular prism deployable mast. *Journal of Astronautics*, 2016, 37(3): 275–281. (in Chinese)
- [25] H Yang, R Q Liu, Y Wang, et al. Experiment and multiobjective optimization design of tape-spring hinges. *Structural and Multidisciplinary Optimization*, 2015, 51(6): 1373–1384.

Submit your manuscript to a SpringerOpen<sup>®</sup> journal and benefit from:

- Convenient online submission
- Rigorous peer review
- Open access: articles freely available online
- High visibility within the field
- Retaining the copyright to your article

---

Submit your next manuscript at ► [springeropen.com](http://springeropen.com)

---